Supplementary information

MNPs capture dynamics

Dynabeads and the MNPs used here are both made from superparamagnetic iron oxide. The magnetic force pulling on those types of particles when subject to an external magnetic field is proportional to the gradient of the magnetic field. To circumvent the need for large external magnets, we and others[1-4] used micropillar arrays or packed iron beads to significantly increase this magnetic field gradient locally and achieve the necessary magnetic force using magnets that can reasonably be mounted on a centrifuge rotor.

The center of the M-Chip array is 7.5 mm away from the surface of the permanent magnet. The length of the magnet provides a semi-uniform external magnetic field across the micro-pillars area. Using a gaussmeter at x_1 = 6.5 mm and x_2 = 10 mm we measure magnetic field values of y_1 = 112 kA/m and y*2* = 82 kA/m and calculated a magnetic field gradient of 8.57 x 10^6 A/m^2. Using an analytical model[2], we calculated the gradient generated by a hollow amorphous Ni cylinder with a Ni shell thickness of 5.5 µm and an internal radius of the polymer based cylinder of 10 µm, yielding a magnetic field gradient of ~10^9 A/m^2.

Using the following constants for core-shell superparamagnetic iron-oxide MNPs and a pillar array coated with amorphous Ni:

Constant	Value
Magnetic moment per unit of mass (from Fonnum et al.[5])	$\rho_M = 10.8\ Am^2/Kg$
Mass density of the particle	$\rho = 1400\ kg/m^3$
Radius of the magnetic particles	$R = 200\ nm$
Saturation magnetization of the Nickel coating (from Malic et al.[2])	$500\ kA/m$
Magnetic pillar internal radius (hole)	$10\ \mu m$
Magnetic pillar external radius (with shell)	$15.5\ \mu m$
Distance from the center of the pillar to the particle	$15.5\ \mu m + 9.5\ \mu m = 25\ \mu m$
Intensity of the external magnetic field	$H_0 = 100\ kA/m$
Capture chamber cross-sectional area	$15\ mm$ by $80\ \mu m$
Capture step flow rate	$Q = 200\ \mu L/min$
Average flow speed in the array	$U = 2.7\ mm/s$

The magnetic moment of one particle is:

$$M_o = \rho_M \rho \frac{4\pi R^3}{3} = 5.1 \times 10^{-16} Am^2$$

The magnetic force acting upon particles is:

$$F_m = \mu_0 M_0 \nabla H = 2.48\ pN$$

With $\mu_0 = 4\pi \times 10^{-7} H/m$ and ∇H the gradient of the magnetic field generated by the pillar. This gradient is calculated analytically in MATLAB.

The Drag force (Stokes) is:

$F_S = 6\pi\eta RU = 10.1\ pN$

And the maximal Drag Force is:

$$F_{Smax} = 1.5 \times F_S = 15\ pN$$

With a flow rate set to 200 µL/min during the MNP capture protocol step, a 400 nm MNP flowing through the *M-Chip* is subjected to a maximal Stokes drag of 15 pN parallel to the flow with a minimal magnetic force of 2.48 pN displacing the MNP perpendicularly to the flow. This configuration ensures that, for a proper liquid flow speed, the MNPs are rapidly trapped on the pillars by the high local magnetic field gradient and experience only minor deviations in trajectory due to the external magnetic field before entering the *M-Chip* array.

Deterministic filling of large microstructured chambers in centrifugal microfluidics

Filling of micro-channels and complex micro-structures is critical for reliable operation of most microfluidic devices. Incomplete filling of structures or trapping of air-bubbles may significantly affect the flow behavior and thus hinder smooth progress of complex biologic protocols. Furthermore, the type of micro-pillar array used in the *M-Chip* belongs to a family of structures which can be particularly challenging to fill under forced flow dynamics and in the presence of multiple interfaces with varying surface tension properties. Indeed, the insert fabrication requires

two materials (COC and TPE) with different surface properties as well as inherently hydrophobic Ni/Au coating on the pillars. The micropillar array used here is 17 mm wide, 5 mm long and 80µm deep (**Fig. S1a**). Filling it properly without significant air bubble trapping requires tight control of the progression of the fluid front which is also challenging wide and shallow chamber. Others have developed advanced filling strategies[6], used surfactants, degassed reagents, optimized microchannels geometries and mechanical bubble traps[7] to address this issue. For the first time, we demonstrate priming of a large micro-pillar array followed by repeated complete fluid exchange which is easily implemented on a centrifugal microfluidics platform. A schematic of the principle and a movie capture taken during the priming process in the magnetic capture subunit are shown on **Fig. S1 b and e**. For better visualization, the *M-Chip* used here did not forego metal plating and red and blue food dyes were used as contrasting agents. First, an aliquot of blue liquid is transferred to the source chamber which begins the priming process. Liquid flow is driven by the centrifugal force and fills the *M-Chip* from the bottom up. The liquid front then rises in a very controlled and uniform way, shaped by the centrifugal force field, as clearly illustrated by its arc shape on **Fig. S1e**. Complete filling of the device is shown in **Fig. S1f**. Subsequently, aliquots of red and blue liquids are transferred sequentially in the source chamber. Fast, total fluid exchanges from blue to red then from red to blue again are depicted in **Fig. S1 f to j**. All aliquots entering the sink chamber were discarded in the waste. A video clip of the complete process is available in the ESI (**Movie Fig. S1**).

Effect of manufacturing variations on flow control inside the *M-Chip*

Liquid flow through the *M-Chip* sub-unit can be precisely tuned by both platform rotation speed (which controls the centrifugal force on the liquids in the source and sink chambers) and negative pressure on the sink chamber. However, the overall flow rate and flow velocity of the suspended MNPs through the microstructured array strongly depend on array impedance which is a direct function of the width of the gap between the pillars. The *M-Chip* fabrication process is subject to minor thermal expansions and contractions during hot-embossing, as well as growth rate variations of the Ni layer during plating. These effects produce small (~1–3 µm) changes in micropillar diameter, altering the width of the gap between pillars. Given that the fluidic resistance of the array scales approximately with the inverse cube of that gap width (w^3), such dimensional deviations can markedly affect the overall fluidic impedance of the device. We evaluated the impact of these variations by fabricating *M-Chips* with a fixed pillar pitch of 50 µm and pillar diameters between

19 and 21 μm, coated with 5–6 μm of Ni and 0.5 μm of Au. This combination produced inserts with inter-pillar gaps ranging from 15 to 21 μm.

Supplementary figures

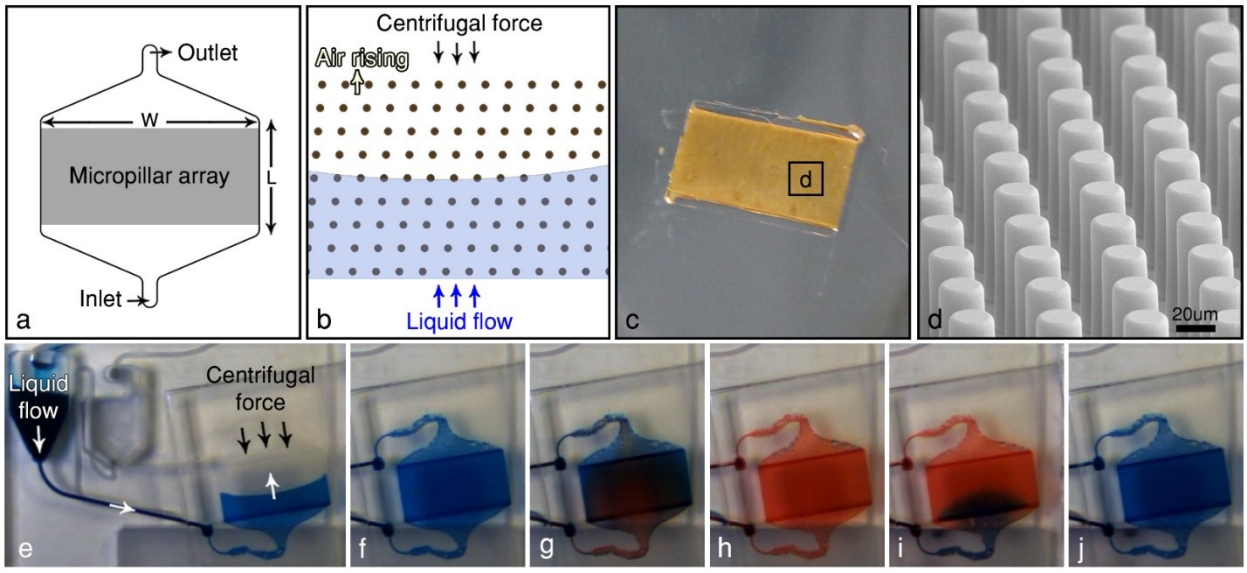

Figure S1: **Deterministic filling dynamics and fluid exchange in a large micropillar array on a centrifugal microfluidics platform.** (a) Design of the magnetic capture insert including a micropillar array and channels connecting it to the main fluidic processor. (b) Geometric configuration of the pillar array and schematic of the filling step against a centrifugal force field. The liquid front is shaped by the centrifugal force. Air rises to the top, avoiding bubble trapping in the array (c) Photograph of a Ni/Au plated M-Chip. (d) SEM micrograph depicting the pillar array inside the M-Chip. Stroboscopic images of (e) the filling step with blue dye. (f) Fully filled micropillar array. (g) to (j) Demonstration of complete fluid exchange without air injection using blue and red dyes.

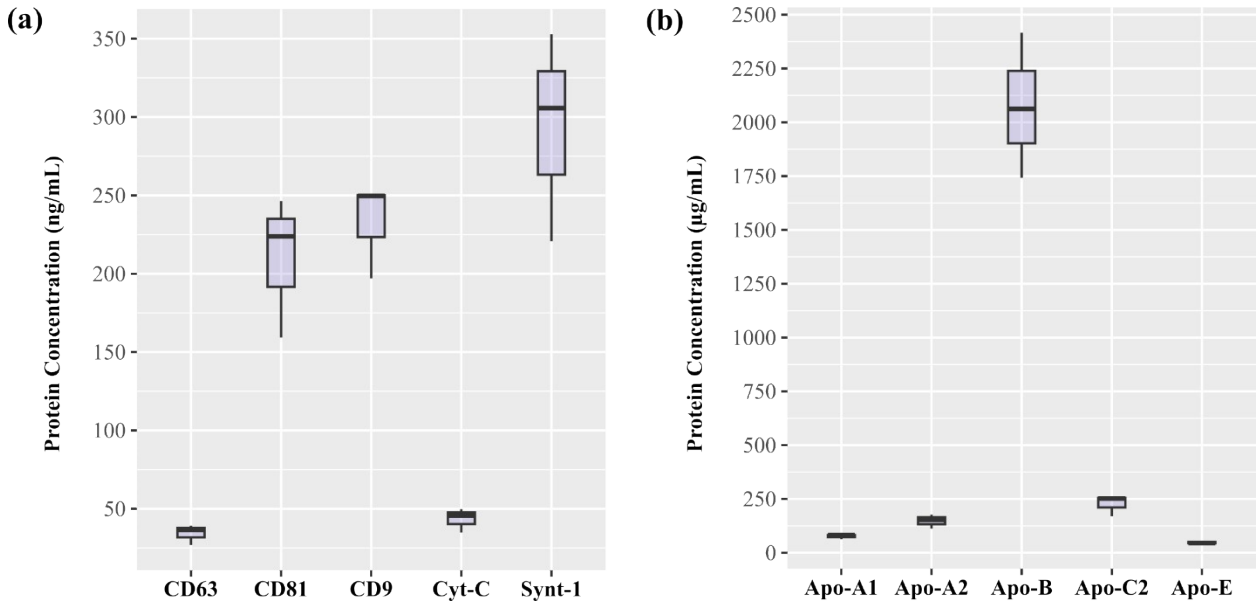

Figure S2: Boxplots of (a) the protein concentrations for known exosomal transmembrane proteins (CD63, CD81, CD9 and Syntenin-1) and the intra-cellular organelle marker Cytochrome-C measured with the ProcartaPlex Exosomes Characterisation Immunoassay in reference PFP samples, (b) lipoproteins concentrations (Apo-A1, Apo-A2, Apo-B, Apo-C2 and Apo-E) measured with the ProcartaPlex Human Apolipoprotein Panel Immunoassay in reference PFP samples.

1. L. Poncelet, L. Malic, L. Clime, M. Geissler, K. J. Morton, C. Nassif, D. Da Fonte, G. Veilleux and T. Veres, *Analyst*, 2021, **146**, 7491-7502.
2. L. Malic, X. Zhang, D. Brassard, L. Clime, J. Daoud, C. Luebbert, V. Barrere, A. Boutin, S. Bidawid, J. Farber, N. Corneau and T. Veres, 2015, **15**, 3994-4007.
3. S. Miltenyi, W. Müller, W. Weichel and A. Radbruch, 1990, **11**, 231-238.
4. H. Fang, M. Liu and W. Jiang, *Applied Biochemistry and Biotechnology*, 2023, **195**, 3109-3121.
5. G. Fonnum, C. Johansson, A. Molteberg, S. Mørup and E. Aksnes, *Journal of Magnetism and Magnetic Materials*, 2005, **293**, 41-47.
6. J. Monahan, A. A. Gewirth and R. G. Nuzzo, *Analytical Chemistry*, 2001, **73**, 3193-3197.
7. I. Pereiro, A. Fomitcheva Khartchenko, L. Petrini and G. V. Kaigala, *Lab Chip*, 2019, DOI: 10.1039/c9lc00211a.